Transient Potential Gradients and Impedance Measures of Tethered Lipid Bilayer Membranes (tBLMs): Pore Forming Peptide Insertion and the Effect of Electroporation

Charles G. Cranfield*†§, Bruce Cornell¶§, Stephan L. Grage‡, Paul Duckworth#, Sonia Carne¶, Anne S. Ulrich‡, and Boris Martinac*†.

*Molecular Cardiology and Biophysics Division, Victor Chang Cardiac Research Institute, 405 Liverpool St, Darlinghurst 2010, NSW, Australia; †St Vincent's Clinical School, University of New South Wales, Sydney 2052, Australia; ¶Surgical Diagnostics Pty Ltd, Unit 6, 30-32 Barcoo St, Roseville 2069, NSW, Australia; ‡Karlsruhe Institute of Technology, Institute of Biological Interfaces (IBG-2), Karlsruhe, Germany; # eDAQ Pty Ltd, 6 Doig Ave, Denistone East, NSW 2112. Australia

§Contributed equally to this paper.

Author for correspondence: c.cranfield@victorchang.edu.au

ABSTRACT

In this work we present experimental data, supported by a quantitative model, on the generation and effect of potential gradients across a tethered bilayer lipid membrane (tBLM) possessing a novel architecture. A challenge to generating potential gradients across tBLMs arises from the tethering coordination chemistry requiring an inert metal such as gold, resulting in any externally applied voltage source being capacitively coupled to the tBLM. This in turn causes any potential across the tBLM assembly to decay to zero in milliseconds to seconds depending on the level of membrane conductance. Transient voltages applied to tBLMs by pulsed or ramped DC amperometry can, however, provide current-voltage (I-V) data that may be used to measure the voltage dependency of the membrane conductance. We show potential gradients in excess of ~150 mV induce membrane defects that permit the insertion of pore forming peptides. A further novelty reported here is the use of real-time modeling of conventional low voltage AC impedance spectroscopy to identify whether the conduction arising from the insertion of a polypeptide is uniform or heterogeneous on scales of nm–μm across the membrane. The utility of this tBLM architecture and these techniques is demonstrated by characterizing the resulting conduction properties of the antimicrobial peptide PGLa.

Keywords: tethered membranes, lipid bilayers, electrical impedance spectroscopy, PGLa.

Abbreviations:

AC: alternating current
BLMs : black lipid membranes
C_c : counter electrode capacitance
C_m: membrane capacitance
C_{ref} : reference capacitance
$C_{s:}$ series capacitance
C_{th}: tethering electrode capacitance
DC: direct current
DphPC: *70%* zwitterionic *C20 diphytanyl-ether-glycero-phosphatidylcholine lipid: 30% C20 diphytanyl-diglyceride ether*
G_m: membrane conductance
GOF: goodness-of-fit

G_{ref} : reference conductance

I-V : current – voltage

MLP: *mobile lipid phase*

PGLa: *peptide with a terminal glycine leucine-carboxyamide*

POPG: *palmitoyl-oleoyl-phosphatidylglycerol*

RC: resistor-capacitor

tBLM : tethered bilayer lipid membrane

INTRODUCTION

Tethered bilayer lipid membranes (tBLMs) typically consist of a lipid bilayer attached by a sulfur-gold chemistry to a thin gold film deposited onto a solid insulating substrate. The advantage of tBLMs is that, unlike patched or so called black lipid membranes (BLMs), tBLMs are stable for months and do not instantaneously fail when subjected to robust mechanical mixing of solutions over their surface or when challenged with transmembrane potentials of greater than ±500 mV (see Fig S1 in Supporting Material).

The tBLMs are fabricated sequentially, starting with a monolayer of sulfur groups that chemically attach to the gold surface and are covalently connected by linkers to hydrophobic groups that tether a subsequently formed lipid bilayer (Fig 1*A*). Following the formation of the monolayer at the gold surface, a further solution of mobile lipids is incubated over the monolayer and following 1-2 minutes is flushed with buffer to form a tethered lipid bilayer. In the current tBLM architecture the sulfur attached monolayer also contains *spacers* that laterally separate the *tethers* but do not directly interact with the membrane (Fig 1*A*). These spacers permit patches of mobile lipid to form within the tBLM into which other molecules such as peptides or proteins may be inserted. For an excellent description of the structural detail of sparsely tethered membranes refer to Heinrich et al 2009 (1).

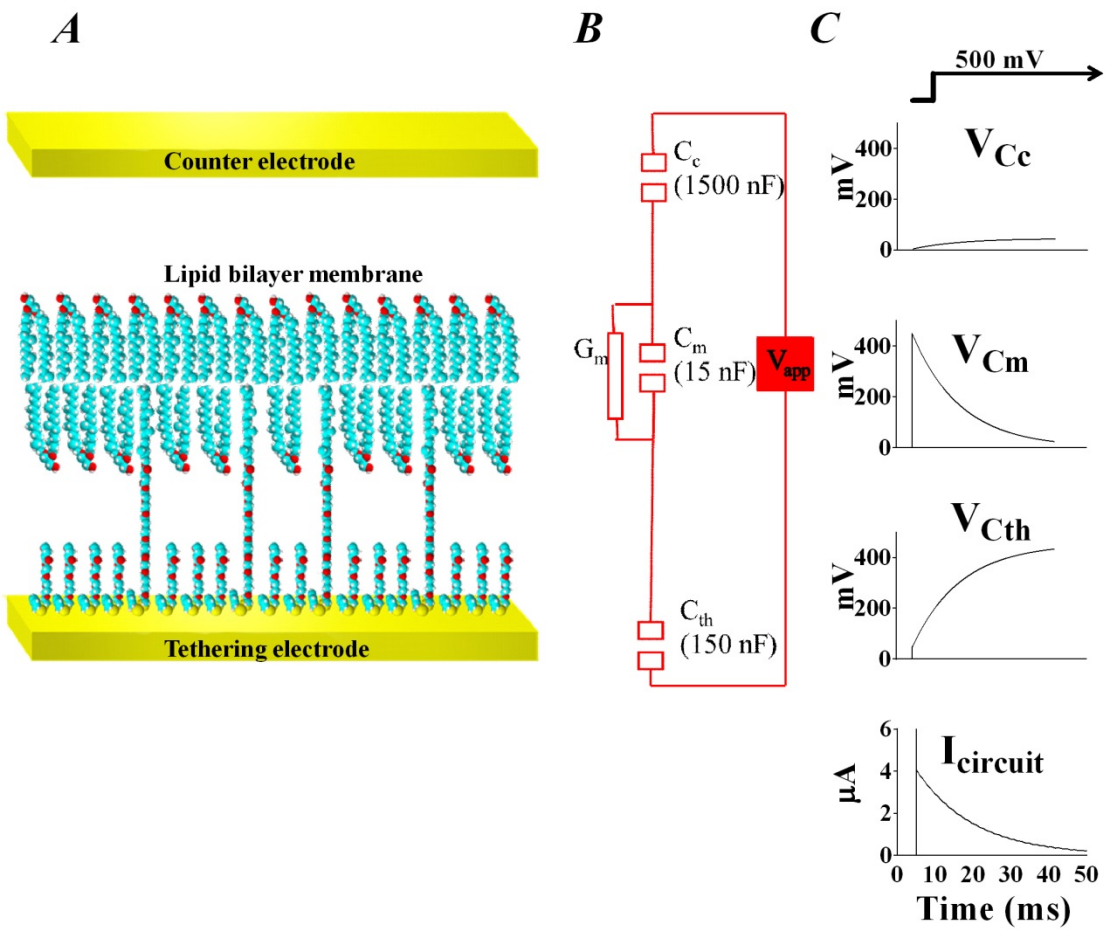

Figure 1, ***A*** Schematic diagram of a typical tBLM used in these experiements. ***B*** The equivalent circuit for the tBLM used here. For the electrode area of 2.1 mm^2 the actual values have been rounded to 1500 nF, 150 nF and 15 nF in order to emphasise the tenfold differences that exists between the capacitance at each layer of the equivalent circuit. ***C*** Of the 500 mV step applied across the whole circuit, ~1% or 0.004504 V is initially expressed across the gold counter electrode $\mathbf{C_c}$; ~10% or 0.04504 V across the tethering gold surface $\mathbf{C_{th}}$; and ~90% or 0.4504 V across the tethered membrane $\mathbf{C_m}$. The current response (bottom) initially shows a capacitive spike due to charging of C_m, C_{th} and C_c. Following this initial spike the current slowly decays due to the charge being redistributed across C_{th} and C_c. When C_{th} and C_c are fully charged the voltage across the membrane and the current will have both decayed to zero.

In the tBLMs used here 10% of the molecules are tethers and 90% are spacers. Using this tether-to-spacer ratio tBLMs may be stored and remain functional for 2-3 months. This is to be contrasted with BLMs which typically have lifetimes of the order of tens of minutes. Furthermore, BLMs are formed using solvents such as squalene or hexane and retain a significant fraction of the solvent within the hydrophobic interior of the bilayer (2). Such retained solvent can significantly alter the membrane properties. In solvent exchanged tBLM's (3), however, the residual solvent levels can be essentially eliminated by aqueous rinsing following membrane formation (see Fig S2 in Supporting Material). Forming a lipid bilayer over the tethered monolayer has most commonly

been accomplished by employing the fusion of liposomes onto the monolayer. This requires a high density of tethers to present a sufficiently hydrophobic monolayer surface to trigger the fusion of the liposomes with the tethers. This limits the fabrication of tBLMs with ratios of tether – to spacer groups above 70 : 30 (4). This approach has its limitations as high tether densities have been shown to increase the membrane thickness (1), and the absence of sufficient patches of mobile lipid, created by the presence of spacer molecules in the monolayer, prevents the inclusion of compounds with a membrane incorporated fraction exceeding ~1 kDa (calculated from the molecular volume (v) assuming a 4 nm thick membrane with the area per lipid being ~1nm^2, where the molecular mass (m) is related to the density (ρ)). At tether densities of 10% sufficiently large mobile lipid patches exist to permit the incorporation of membrane embedded protein fractions possessing molecular weights up to ~40 kDa. Tether densities as low as 1% have also been shown to possess stabilities of up to a month (Fig S3 in Supporting Material) and can provide mobile lipid spaces that are sufficiently large to permit the insertion of membrane bound protein fractions of up to ~300 kDa.

In the tBLM architecture described here benzyl disulfide groups are employed as the sulfur chemistry for attaching the monolayer to the gold surface. Two families of benzyl disulfide terminated groups are used, one possessing a four oxygen-ethylene glycol group terminated by an OH group, which is included as the *spacer* molecule, and a second possessing an eight oxygen-ethylene glycol group terminated by a single chain C20 hydrophobic phytanyl chain included as the *tether*. The C20 phytanyl chain incorporates into the inner leaflet of the subsequently formed lipid bilayer and tethers the bilayer to the gold surface.

Disulfide groups were chosen to minimize the effects of oxidation on the starting materials. Thiols tend to oxidize to disulfides on storage which can cause the composition of the sulfur layer to vary. Disulfides do not suffer this problem. Here, the use of *benzyl* disulfides provides two additional advantages; they strengthen the weaker disulfide-gold bond through the dispersive attraction of the benzyl ring to the gold, and act as an additional class of lateral spacer. The benzyl groups separate the gold attachment points at the sulfur-gold interface creating volume that increases the mobility of ions adjacent to the gold. Ion mobility is ~~a~~ key to the use of tBLMs as a model for mimicking biological membranes and the inclusion of an aqueous space between the gold surface and the tethered membrane provides a reservoir in which ions crossing the membrane may be stored or returned to the external solution (4-6). The fact that the spacer molecules used here are only half the length of the tether molecules creates an increased volume in the reservoir space, further increasing the mobility of ions in the reservoir and relaxing any packing restrictions

experienced by the mobile lipid molecules within the tethered bilayer. The additional volume within the reservoir provided by the shorter spacer molecules also relieves steric interferences that might arise from protein moieties that project beyond the lipid bilayer.

A challenge to studying the effects of transmembrane voltages across the tBLM arises from the isolation of the tBLM caused by the capacitive property of the gold surface to which the membrane is tethered. Any conductance across the tBLM will discharge the voltage across the membrane. In the architecture described here (Fig 1*B*) a fixed potential, V, applied to the tBLM circuit initially applies ~90% of V across the tBLM itself and ~10% of V across the tethering and return gold electrodes. The potential across the tBLM will decay over milliseconds to seconds, discharging the voltage to zero whilst simultaneously charging the tethering and return electrode capacitors to ~90% of V and ~10% of V respectively. The voltages throughout this process reflect the inverse relationship of V with the capacitance values of the membrane, C_m, the tethering gold surface, C_{th}, and the return or *counter* electrode, C_c (Figs 1*B* & 1*C*). Connecting the membrane directly to the voltage source, rather than through capacitive coupling by using redox active electrodes might be thought as an alternative approach. However, if redox active metals are used at the *tethering* electrode, the metal will ablate causing a release of the tethers and a destabilization of the membrane. Furthermore, the use of a redox active *counter* electrode will result in the release of metal ions into the bathing solution potentially inactivating proteins or peptides being studied in the tBLM (7).

Using a tBLM with electrochemically inert gold electrodes, applied pulsed or ramped voltages will sustain transmembrane potentials for times in the range of 1 ms – 100 ms across the membrane with typical conductances, G_m, of 100 μS cm^{-2} – 1 μS cm^{-2} respectively. From the I-V relationship in these time windows, studies may be undertaken of the voltage dependency of the insertion of peptides or ionophores into tBLMs, and of the intrinsic dependency of conduction of an ionophore once formed within the membrane.

The actual potential gradient across the tBLM may be quantitatively measured as a function of time from C_s, the effective series capacitance of C_{th} and C_c given by Equation 1 and the integrated current as a function of time flowing through G_m. At any instant, *t*, the loss of voltage across the tBLM is matched quantitatively by the voltage increase across C_s.

$$C_s = {C_c C_{th}}/{(C_c + C_{th})} \qquad \mathbf{1}$$

The voltage increase is given by Q/C_s where Q is the integral of the discharge current I, accumulated to that point in time, *t*.

The ability of tBLMs to withstand high potentials provides a unique model for the study of the effects of electroporation membrane damage. Here we propose that one result of electroporative failure is an increase in the membrane insertion efficiency of peptides. Peptides will spontaneously insert into lipid bilayers at zero applied potential, but the efficiency of insertion is increased by many orders of magnitude if membrane defects have been formed by electroporation. In the present study, the insertion, assembly and conduction of the antimicrobial peptide with a terminal glycine leucine-carboxyamide (PGLa) was observed whilst applying both pulsed and ramped potentials to tBLMs possessing 10% tethers and 90% spacers.

Using a unique AC impedance spectroscopy method, the spontaneous insertion level of PGLa was measured at zero net transmembrane potential. This AC impedance spectroscopy method described here fits the impedance data in real time against an idealized single capacitor – single resistor circuit. This real-time modeling of the AC impedance data suggests that the origin of the loss of PGLa conduction at long times (hours) can be attributed to the formation of peptide aggregates forming in the membrane, which reduces the conduction per peptide and creates an inhomogeneous membrane.

MATERIALS AND METHODS

Tethered Membrane Formation

tBLMs were made using pre-prepared tethered *benzyl-disulfide ethylene glycol* "T10" coated gold slides including 10% *eight oxygen ethylene glycol* reservoir linkers with a *C20 phytanyl* group as *tethers* and 90% *four oxygen ethylene glycol* reservoir linkers with a terminal *OH* group as *spacers* (SDx Tethered Membranes Pty Ltd, Australia; Fig S4 in Supporting Material). A lipid bilayer was formed over the monolayer using a solvent exchange technique employing ethanol and water (3). 8 μL of a 3 mM solution of a mobile lipid phase (MLP) [*70%* zwitterionic *C20 diphytanyl-ether-glycero-phosphatidylcholine lipid: 30% C20 diphytanyl-diglyceride ether*] (DphPC) dissolved in ethanol was added to a 1 μL flow cell chamber with a 500 μl connected liquid storage chamber. After a ~2 min incubation at 20°C they were rinsed with 3 x 100μL of PBS solution. Six such chambers were prepared in a single *tethaPlate*™ cartridge (SDx Tethered Membranes Pty Ltd, Australia). Although many lipid solvents may be used (3, 8), in most instances the mobile lipids chosen to form the bilayer are soluble in ethanol. For lipids such as phosphatidylinositol that are insoluble in 100% ethanol, chloroform, methanol, water mixtures have been used (9).

The formation of the tBLMs was initially tested using a *tethaPod*™ (SDx Tethered Membranes Pty Ltd, Australia) operating as described in the *AC impedance spectroscopy* section below. Typical results obtained for a lipid membrane were 0.8 - 1.2 μF cm^{-2}, and a conduction of 0.3-0.5 μS, for a 2.1 mm^2 area electrode at 20°C and pH 7.2. In order to generate negatively charged lipid bilayers the ethanolic MLP lipid solution was mixed with either 0 - 50% *palmitoyl-oleoyl-phosphatidylglycerol* (POPG).

AC impedance spectroscopy

The conductance and capacitance of the tethered membrane were determined using a *tethaPod*™ conductance reader (SDx Tethered Membranes Pty Ltd, Australia), employing real time modeling of the tBLM whilst operating as a swept frequency ratiometric impedance spectrometer. A sequential 20 mV excitation was applied over the frequency range of 1000Hz, 500Hz, 200Hz, 100Hz, 50Hz, 20Hz, 10Hz, 5Hz, 2.5Hz, 1.25Hz, 0.5Hz, 0.25Hz and 0.125Hz. The substantially capacitive load of a tBLM poses a challenging requirement for direct swept frequency measurements of impedance over four decades of dynamic range necessitating a high digital and analog resolution for the current detection amplifiers. These specifications were relaxed by employing a *ratiometric* measurement.

Ratiometric measure

By measuring the frequency dependence of the potential across the tBLM as a fraction of the applied potential across the tBLM plus a series reference element (Fig 2), a frequency dependent attenuation factor ($f_{attn}(\omega)$) is defined. The series reference element comprises a fixed capacitor in parallel with a resistor with values chosen to be within a similar range to those anticipated in the test tBLM.

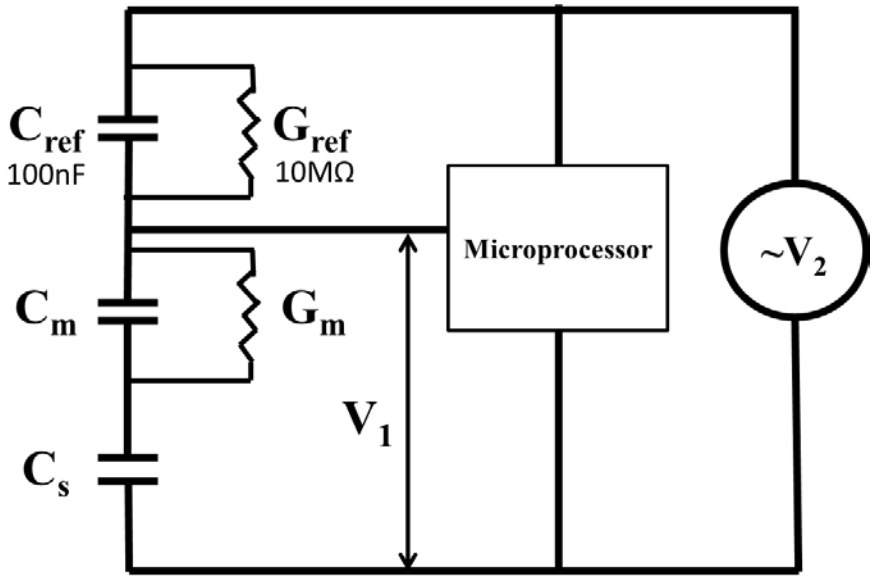

Figure 2, The equivalent circuit used for modeling the goodness of fit values from impedance spectroscopy data. V_2 is a measure of the potential applied across the *total* network impedance, and V_1 is the resultant potential across the unknown *load* impedance.

Fig 2 shows a reference RC network in series with the test tBLM and the coupling capacitor (C_s). The *ratiometric* approach results in a reduction by two orders of magnitude of the required dynamic range to read the impedance data. From the network in Fig 2, C_m, G_m and C_s are fitted by a microprocessor (ADuC70/24, Analog Instruments, USA) to $f_{attn}(\omega)$ according to:

$$f_{attn}(\omega) = {}^{V_1}/_{V_2} = {}^{I * Z_1}/_{I * Z_2} = \sqrt{\frac{(a_l d_l + b_l e_l)^2 + (d_l b_l - a_l e_l)^2}{(e_l{}^2 + d_l{}^2)}} \Bigg/ \sqrt{\frac{(a_t d_t + b_t e_t)^2 + (d_t b_t - a_t e_t)^2}{(e_t{}^2 + d_t{}^2)}} \qquad \mathbf{2}$$

where V_1 and V_2 are the potentials across the unknown *load* impedance (Z_1) and across the *total* network (Z_2), respectively, and *I* is the current through the network. The constants *a*, *b*, *d* and *e* relate to the total (*t*) network impedance and the load (*l*) network impedance, whilst ω is the excitation frequency in radians per second.

i.e., for the *total* impedance network including reference and unknown load:

$$a_t = 1 - \frac{\omega^2 (C_m C_s + C_{ref} C_m + C_{ref} C_s)}{G_m G_{ref}} \quad \textbf{3}$$

$$b_t = \omega\left(\frac{C_s}{G_{ref}} + \frac{C_s}{G_m} + \frac{C_{ref}}{G_{ref}} + \frac{C_m}{G_m}\right) \quad \textbf{4}$$

$$d_t = -\omega^2 C_s\left(\frac{C_{ref}}{G_{ref}} + \frac{C_m}{G_m}\right) \quad \textbf{5}$$

$$e_t = \omega C_s - \left(\frac{\omega^3 C_{ref} C_m C_{th}}{G_{ref} G_m}\right) \quad \textbf{6}$$

And for the *load network* impedance (just unknown load):

$$a_l = 1 \quad \textbf{7}$$

$$b_l = \omega\left(\frac{C_s}{G_m} + \frac{C_m}{G_m}\right) \quad \textbf{8}$$

$$d_l = \frac{-\omega^2 C_s C_m}{G_m} \quad \textbf{9}$$

$$e_l = \omega C_s \quad \textbf{10}$$

Goodness of fit.

The frequency dependence of the experimental attenuation factor is compared in real time during data acquisition with the calculated value according to Equation 11. This approach tests the ability of the data to be mimicked by an idealized homogeneous conducting membrane modeled as a single membrane capacitance (C_m) in parallel with a single membrane conductance (G_m). The goodness of fit (GOF) function,

$$\text{GOF} = \sum_{\omega=2\pi 0.1}^{\omega=2\pi 1000} \sqrt{\left(f_{attn\,(\omega)_{experimental}} - \mathrm{f}_{attn\,(\omega)_{model}}\right)^2} \quad \textbf{11}$$

is minimized within the *tethaPod*™ by adjusting C_{th} C_m and G_m, whilst maintaining C_{ref} and G_{ref} fixed at C_{ref} = 100 nF cm^{-2}, and G_{ref} = 0.1 µS. The RMS differences across all frequencies

are summed, and if found to be ≤ 0.1, the values of G_m and C_m used in fitting the experimental data are reported.

A significant deviation of the data from the homogeneous membrane model indicates the conductance arises from multiple C_m and G_m values, distributed at different sites across the membrane. This may occur physically from the aggregation of conductive pores into patches on a scale of 10's – 100's of nanometers defined by the diffusion distance of a conductive ion during the period of the AC electrical excitation. An alternative interpretation is that an increase in GOF arises from a patchy loss of the membrane integrity due to, for example, detergent action or voltage breakdown causing well separated areas of membrane to degrade. Under these latter circumstances, however, the increase in the GOF is likely to be associated with a significant increase in the membrane capacitance (C_m) as more of the inner tethering surface capacitance is revealed. This was not generally observed here, suggesting that the reported effects arise from aggregation or clustering of the inserted peptides.

DC Pulsed potential gradients

Voltage transients were applied across the tethered membrane circuit using an eDAQ ER466 Potentiostat in conjunction with *eScope* software (eDAQ Pty Ltd, Australia) operating with a bandwidth of 100 kHz. Rectangular voltage pulses were applied of 20 ms duration, increasing from 0 mV to ±300 mV in 50 mV increments (Fig 5*A*). Simultaneous current recordings were averaged over 16 sweeps with a repetition delay of 1 s. Potentials are defined as the potential of the tethered gold electrode relative to the return electrode. Following all potential measurements up to ±300 mV, any lasting damage caused to the tBLMs was determined using AC impedance spectroscopy. In order to induce lasting electroporation damage, three sequences of 20 ms pulses, ten steps each from 0 to ±500 mV in ±50mV increments were applied.

Ramped potential gradients

Ramped potentials were applied using *EChem* v4.0.13 software (eDAQ Pty Ltd, Australia). Voltage ramps of ±100 V/s were applied for 3 ms, to a peak of ±300mV. Voltage increases occurred stepwise in 100 x 0.05 ms steps (i.e. ±5mV/0.05 ms). For each 0.05 ms step, current recordings were averaged over 0.01 ms intervals following the voltage increment. It was important to limit the time course of the potential ramps to less than a few milliseconds in order to ensure the transmembrane potential closely matched the applied potential ramp.

Antimicrobial peptide PGLa synthesis

The peptide GMASKAGAIAGKIAKVALKAL-amide (peptidyl-glycine-leucine-carboxyamide (PGLa)) was synthesized using standard solid-phase Fmoc protocols (10, 11) on an *Applied Biosystems* 433A instrument, and purified using reverse phase HPLC employing a water/acetonitrile gradient and a C18 column as described in detail by Afonin et al (12). The bacterial toxin channel α-hemolysin was purchased from *Sigma-Aldrich*.

Equivalent Circuit Modeling

The electrical equivalent circuit of the 2 mm^2 tethered membrane experimental system for both AC impedance spectroscopy and DC amperometry is shown in Fig 1*B*. The response of this circuit to any applied potential may be simulated using the freeware simulation package *5SPICE* (Andresen Software, USA). The circuit comprises two coupling capacitors [~70 µF cm^{-2} return electrode (C_c); ~7 µF cm^{-2} gold tethering electrode (C_{th})] and a 0.8 - 1.2 µF cm^{-2} membrane capacitance (C_m). In addition, it contains a conductor (G_m), representing the membrane conduction whose value may be adjusted to represent the conductivity of an ion channel, or in the absence of an ion channel, the baseline conduction of the tethered lipid bilayer. Circuit responses across all elements for pulsed and ramped applied potentials are shown in Fig 1*C* and Fig 6*B* respectively.

RESULTS

Effect of PGLa addition on conductance measured by AC impedance spectroscopy

The *tethaPod*™ reader provides a continuous recording of G_m and C_m based on fitting the impedance spectrum to a single idealized G_m - C_m network together with a GOF value indicating the quality of the fit of the data to this simple equivalent circuit. Fig 3*A* shows G_m during the addition of 10 µL of varying concentrations of PGLa in PBS. Fig 3*B* is the peak conduction in Fig *3A* which shows a nonlinear relationship with PGLa concentration. Fig *3C* shows the conductance following the addition of 30 µM PGLa to membranes that contain 0% to 50% of the negatively charged phospholipid POPG in PC lipids. The peak conductance progressively increased more than thirtyfold by progressively increasing the POPG concentration. However at longer times the G_m response to PGLa, in either PC or POPG enriched tBLMs, reversed and decreased. The bacterial toxin α-Hemolysin is included as a control in Fig *3C*. Unlike the effect

of PGLa on conductance, α-Hemolysin caused a conductance increase that remained high, and even slightly increased over five hours.

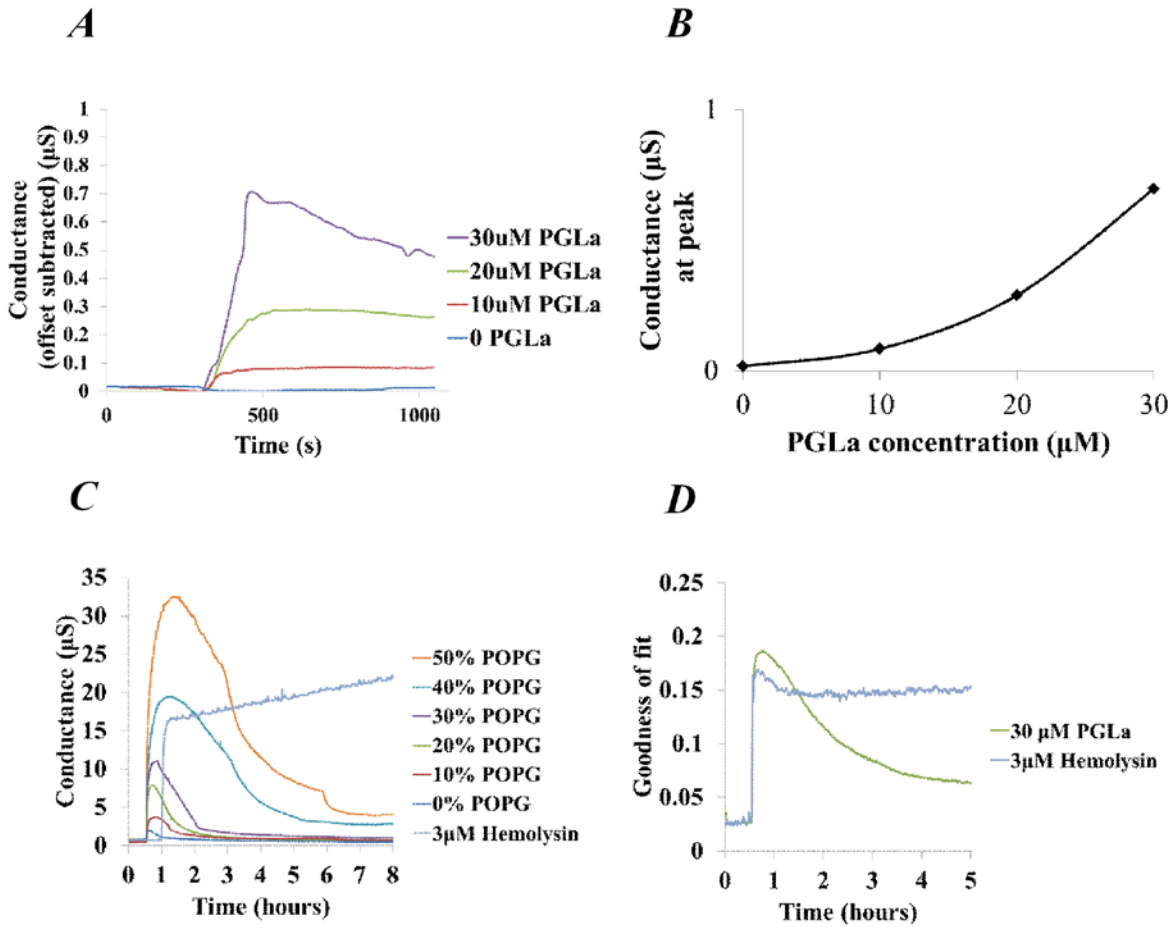

Figure 3, ***A*** AC impedance spectroscopy conductance readings in response to varying concentrations of PGLa in zwitterionic lipids over time. All readings were baseline conductance offset from the time-point at addition of a 10µL PGLa sample or a blank PBS control. ***B*** Peak conductance readings from ***A*** for each PGLa concentration. ***C*** AC Impedance spectroscopy conductance readings of 30 µM PGLa added to tBLMs containing various amounts of negatively charged POPG lipids. PGLa responses are compared to the addition of 3µM α-hemolysin to a POPG-free tBLM. ***D*** AC impedance goodness of fit (GOF) calculations in response to PGLa and α-hemolysin over time.

Membrane Heterogeneity

With the rise in conduction due to the addition of PGLa there is an associated and progressive increase in the GOF beyond 0.1 indicating the failure of the single C_m and single G_m network model to describe the impedance characteristics of the membrane. This suggests a progressively more heterogeneous distribution of conductive PGLa within the membrane as the conduction increases. The origin of this heterogeneity may arise from PGLa self-assembling and/or forming mixtures with the anionic lipids (13). As the conduction decreased, the GOF

also decreased suggesting the reduction in G_m was associated with an annealing of the heterogeneities giving rise to a more homogenous and less conducting state. Salnikov and Bechinger (2011) and reported multiple conformations of PGLa are adopted within a lipid bilayer at high concentrations of PGLa (14). These multiple conformations may reflect states with different conductivity such as those seen here. The bacterial toxin α-hemolysin similarly causes the GOF to increase with conduction however, with α-hemolysin the raised conduction and GOF are maintained over many hours (Fig 3*D*). Modeling the effect of peptide insertion on the heterogeneity of membrane conduction can be pursued using more complex constant phase element (CPE) models (15), but is beyond the scope of the current discussion.

Membrane Capacitance

Fig 4 shows C_m as a function of percentage POPG content in DphPC tBLMs. The incorporation of POPG into the tBLM is evident from the linearity of the capacitance change with the nominal POPG content.

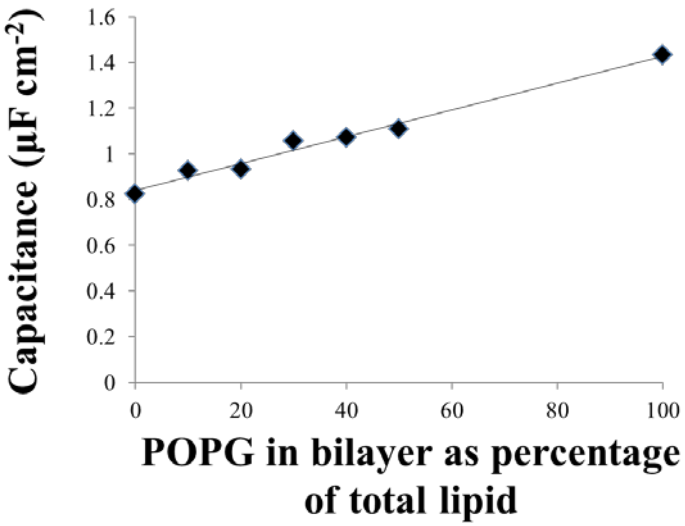

Figure 4 Increased capacitance caused by incorporating the anionic POPG into the lipid bilayer.

Electroporation

Fig 5*A* shows applied voltage steps (V_{app}) in the range 0 – ±300 mV in 50 mV steps across a tBLM containing 40% POPG lipids. The current traces possess an initial short-lived high

amplitude spike, followed by a series of low amplitude exponential decays that continued beyond the measurement period of 20 ms. These current traces reflect the inherent charging current of C_s through $G_{m.}$ The integral of this current is a measure of the charge ($Q_{(t)}$) being transferred across the membrane. The voltage across the membrane $V_{m(t)}$ is thus given by the applied voltage minus $Q_{(t)}/C_s$:

$$V_{m(t)} = V_{app} - \frac{Q_{(t)}}{C_s} \qquad \mathbf{12}$$

At voltages greater than ~150 mV the current traces diverge from a linear dependence on voltage suggesting an increased current due to electroporation (Fig 5*B*). This is more evident in the presence of the peptide PGLa, suggesting that electroporation assists with peptide insertion. Fig 5*C* shows the normalized $V_{m(t)}$ at V_{app} of 50 mV and 300 mV. The electroporation caused by V_{app} = 300 mV results in a more rapid decay of $V_{m(t)}$ than with V_{app} = 50 mV.

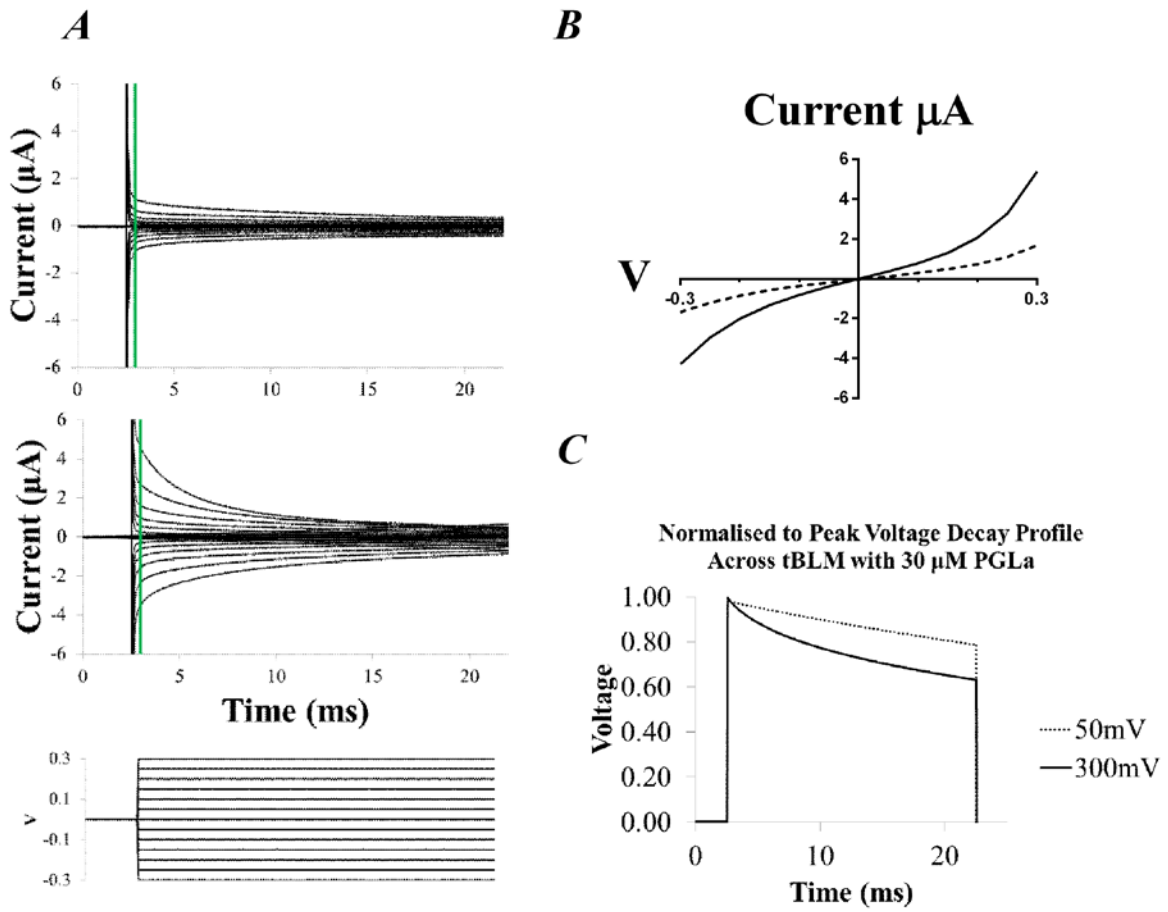

Figure 5, ***A*** Voltage clamp data measured from a tethered lipid bilayer containing 40% negatively charged POPG lipids in the absence (top) and presence of 30µM PGLa peptide (bottom). 50 mV voltage steps were applied for 20 ms (bottom plot). Recordings at each voltage step are the average of 16 sweeps. Green lines indicate time periods of 0.3 ms post pulse initiation. ***B***, I-V plot of responses recorded 0.3 ms post pulse initiation for control (dashed line) and in response to 30µM PGLa (solid line). At voltages greater than ~150 mV the current traces become non-linear suggesting an increased current due to electroporation. This is clearly evident in the PGLa case indicating that electroporation assists with peptide insertion ***C*** By integrating the data from the pulsed traces in ***A*** it is possible to calculate the charge across the membrane, and thereby the voltage across the membrane. The plot in ***C*** represents the normalized to peak voltage decay across the membrane to an applied 20 ms pulse of 300 mV compared to a 50 mV pulse of the same duration. Because of electroporation, a more rapid decay in voltage across the membrane is seen due to decreased resistance across the tBLM than at lower voltages.

The application of a linear voltage ramp in the same range of 0 - ±300 mV showed a current trace reflecting a similar dependency of electroporation on voltage as that seen with the application of pulsed potentials. A 5SPICE simulation of ramped potentials across the equivalent circuit is shown in Fig 6*B*. The simulated step in current with the onset of the

potential ramp closely matches the experimental result confirming the AC impedance measurement of C_m = 1.19 µF cm^{-2}. In Fig 6C the current trace with and without PGLa is compared with the equivalent circuit. However, in this case, the tBLM had been subjected to multiple voltage steps between ±500 mV resulting lasting electroporation damage which potentiated the effects of PGLa on the transmembrane current.

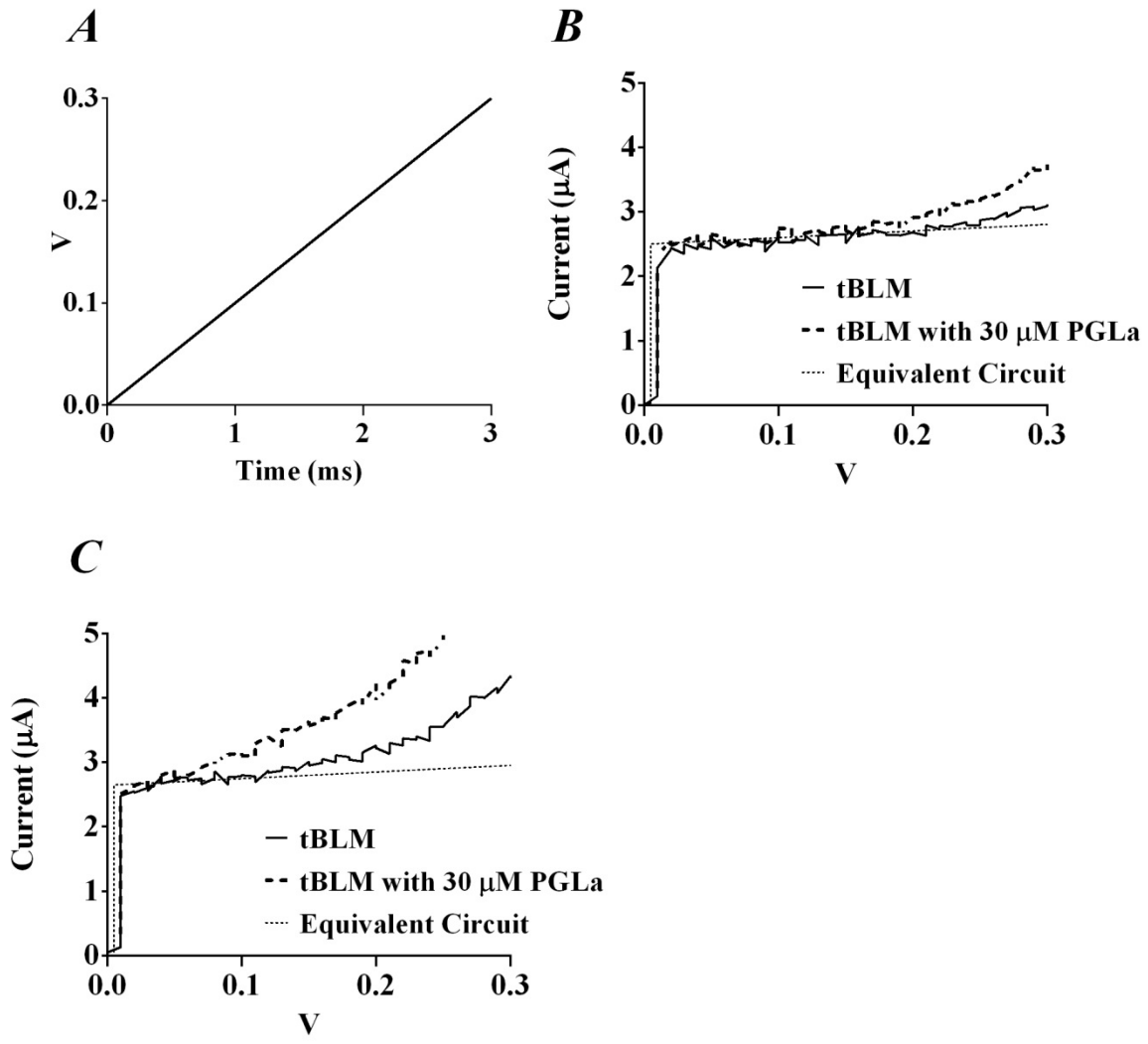

Figure 6 ***A*** Ramped voltage pattern applied to the tBLM to measure the electroporation threshold. ***B*** The resultant current in response to the voltage ramp illustrates the electroporation threshold, and the insertion of PGLa compared with the experimental current and a 5SPICE simulation of the equivalent circuit of a sealed tBLM. The initial rise in current seen in both the experimental and simulated traces confirm the capacitance readings obtained using AC impedance spectroscopy of C_m = 1.19 µF cm^{-2}. ***C*** A further tBLM after exposure to 3 sequences of 20 ms pulses from 0 to ±500 mV in ±50mV increments, and subsequently read using the same ramped potential as in ***B***. It should be noted that the S/N ratio of the currents measures arising from the ramped potentials in Fig 6*B&C* is approximately 1-2 orders of magnitude lower than that from the swept frequency AC measures.

DISCUSSION

The tBLM architecture employed here incorporating sparsely separated tethering sites permitted the incorporation and formation of conductive membrane defects induced by PGLa. The tethered membranes could be prepared incorporating up to 100% charged POPG lipids, allowing the study of the influence of charged lipids that mimic bacterial membranes.

Two approaches have been applied here to study the incorporation of the antimicrobial peptide, PGLa, into tBLMs. A low voltage (20 mV) AC impedance spectroscopy reading provided measures of basal membrane conduction and capacitance; and a high voltage (0 – ±300 mV) pulsed and ramped amperometry approach provided measures of the electroporation voltage dependency of the membrane ~~in terms of~~ catalyzing PGLa incorporation and conduction. The non-linearity of the peak conduction as a function of PGLa concentration suggests that some level of oligomerization of PGLa is required to form a conductive pore, as has been suggested previously for similar antimicrobial peptides (16, 17).

The conductance increase that was observed upon the addition of PGLa to the membrane correlates with an increased GOF value. This may arise from the formation of families of conductive PGLa aggregates ~~trans~~ possessing a number of different membrane topologies (14, 18). However, even though the membrane conduction is heterogeneous, the capacitance remained substantially unaltered, indicating that the membrane remained intact (see Fig S5 in Supporting Material). The speed at which the impedance spectrum changes upon the addition of PGLa can have an impact on the apparent estimate of GOF. Transients in conduction that are faster than the sweep rate from 1000 Hz to 0.1 Hz (~20 sec^{-1}) will result in GOF estimates that will yield flawed measures of G_m, C_m and C_c. In the current data, such transients are evident immediately upon the addition of PGLa, but are relaxed within less than 1 min as the rate of change of conductance decreases below the data acquisition rate (data not shown).

Following the application of a 20 ms DC potential pulse of increasing magnitude, the resultant current decay could be decomposed into multiple components. The transmembrane potential is significantly reduced after 15 – 20 ms as the coupling capacitors C_{th} and C_c are charged through the membrane conductance $G_{m.}$ At low voltages (less than ~±150 mV), the dominant feature is a rapidly decaying spike (0.5 ms) arising from a large displacement current charging both the membrane and coupling capacitors. At longer times, a current consistent with the

measured AC conductance levels persisted beyond 20 ms. At higher voltages (greater than ±150 mV), an additional current component decaying over 15 ms became evident and was identified with electroporation defects caused by the voltage pulse sustaining the membrane voltage above a critical electroporation threshold.

In the presence of PGLa similar characteristics were observed, except that with the onset of electroporation the current was significantly greater and the long-term conduction remained higher. This is interpreted as the electroporation facilitating the incorporation of PGLa, which then results in an increase in long-term membrane conduction.

An electroporation threshold potential may be determined more readily from the *ramped* potential data obtained with and without PGLa (Fig 6*B*). Voltages in excess of ~150 mV appeared to form electroporation defects in the membrane that facilitate the formation of PGLa induced pores. Multiple applications of the potential gradient in excess of ±200 mV were required to achieve a sustained high conduction arising from the peptide insertion into the tBLM. With minimal electroporation damage, the raised conduction levels returned to near their initial values. However, with increased electroporation damage, the rise in conduction was sustained (Fig 6*C*). This suggests electroporative pore formation initially causes a reversible insertion of PGLa, but with repeated application of the ramped potential, a sustained conduction is maintained suggesting the membrane included PGLa adopts a new configuration that remains within the membrane when the applied potential is removed.

CONCLUSIONS

In the present study we describe a tBLM architecture and AC impedance spectroscopy technique that allows a rapid measure of the insertion and aggregation of pore forming peptides such as PGLa. The stability of the tethered lipid bilayers also permits the use of high voltage DC amperometry to study electroporation induced defects in the membrane that catalyzed the insertion of PGLa.

ACKNOWLEDGMENTS

This study was supported by National Health & Medical Research Council (NH&MRC) of Australia (Grant 635525). Bruce Cornell is a shareholder, and Sonia Carne an employee, of Surgical Diagnostics Pty Ltd. Paul Duckworth is an employee of eDAQ Pty Ltd. We gratefully acknowledge Parvesh Wadhwani, Andrea Eisele and Kerstin Scheubeck (Karlsruhe Institute of

Technology) for providing the PGLa peptide and the DFG-CFN (TP E1.2) for financial support.

REFERENCES

1. Heinrich, F., T. Ng, D. J. Vanderah, P. Shekhar, M. Mihailescu, H. Nanda, and M. Lösche. 2009. A New Lipid Anchor for Sparsely Tethered Bilayer Lipid Membranes†. Langmuir 25:4219-4229.
2. Cornell, B. A. 2002. Memembrane-based Biosensors. In Optical Biosensors: Present and Future. F. Ligler, and C. A. R. Taitt, editors. Elsevier Science B.V, Amsterdam. 457-459.
3. Cornell, B. A., V. L. B. Braach-Maksvytis, L. G. King, P. D. J. Osman, B. Raguse, L. Wieczorek, and R. J. Pace. 1997. A biosensor that uses ion-channel switches. Nature 387:580-583.
4. Krishna, G., J. Schulte, B. A. Cornell, R. J. Pace, and P. D. Osman. 2003. Tethered Bilayer Membranes Containing Ionic Reservoirs: Selectivity and Conductance. Langmuir 19:2294-2305.
5. Krishna, G., J. Schulte, B. A. Cornell, R. Pace, L. Wieczorek, and P. D. Osman. 2001. Tethered Bilayer Membranes Containing Ionic Reservoirs: The Interfacial Capacitance. Langmuir 17:4858-4866.
6. Cornell, B. A., G. Krishna, P. D. Osman, R. D. Pace, and L. Wieczorek. 2001. Tethered-bilayer lipid membranes as a support for membrane-active peptides. Biochemical Society transactions 29:613-617.
7. Ghandour, W., J. Hubbard, J. Deistung, M. Hughes, and R. Poole. 1988. The uptake of silver ions by Escherichia coli K12: toxic effects and interaction with copper ions. Applied microbiology and biotechnology 28:559-565.
8. McGillivray, D. J., G. Valincius, D. J. Vanderah, W. Febo-Ayala, J. T. Woodward, F. Heinrich, J. J. Kasianowicz, and M. Löscheb. 2007. Molecular-scale structural and functional characterization of sparsely tethered bilayer lipid membranes. Biointerphases 2:21-33.
9. Shekhar, P. 2012. Neutron Reflectometry from Interfacial Molecular Architectures : Structural Modeling and Application to Sparsely Tethered Bilayer Lipid Membranes. In Department of Physics, Pittsburgh, Pennsylvania. Carnegie Mellon University. p113.
10. Chang, C.-D., and J. Meienhofer. 1978. Solid-phase pepetide syntheisi using mild base cleavage of Nα-Fluorenylmethoxycarbonyl amino acids, exemplified by a synthesis of Dihydrosomatostatin. International Journal of Peptide and Protein Research 11:246-249.
11. Fields, G. B., and R. L. Noble. 1990. Solid phase peptide synthesis utilizing 9-fluorenylmethoxycarbonyl amino acids. International Journal of Peptide and Protein Research 35:161-214.
12. Afonin, S., R. W. Glaser, M. Berditchevskaia, P. Wadhwani, K.-H. Gührs, U. Möllmann, A. Perner, and A. S. Ulrich. 2003. 4-fluorophenylglycine as a label for 19F NMR structure analysis of membrane-associated peptides. Chembiochem : a European journal of chemical biology 4:1151-1163.
13. Wadhwani, P., R. F. Epand, N. Heidenreich, J. Bürck, A. S. Ulrich, and R. M. Epand. 2012. Membrane-Active Peptides and the Clustering of Anionic Lipids. Biophysical Journal 103:265-274.

14. Salnikov, Evgeniy S., and B. Bechinger. 2011. Lipid-Controlled Peptide Topology and Interactions in Bilayers: Structural Insights into the Synergistic Enhancement of the Antimicrobial Activities of PGLa and Magainin 2. Biophysical Journal 100:1473-1480.
15. Chang, W. K., W. C. Wimley, P. C. Searson, K. Hristova, and M. Merzlyakov. 2008. Characterization of antimicrobial peptide activity by electrochemical impedance spectroscopy. Biochimica et Biophysica Acta (BBA)-Biomembranes 1778:2430-2436.
16. Yang, L., T. M. Weiss, R. I. Lehrer, and H. W. Huang. 2000. Crystallization of Antimicrobial Pores in Membranes: Magainin and Protegrin. Biophysical Journal 79:2002-2009.
17. Zasloff, M. 2002. Antimicrobial peptides of multicellular organisms. Nature 415:389-395.
18. Glaser, R. W., C. Sachse, U. H. N. Dürr, P. Wadhwani, S. Afonin, E. Strandberg, and A. S. Ulrich. 2005. Concentration-dependent realignment of the antimicrobial peptide PGLa in lipid membranes observed by solid-state 19F-NMR. Biophysical journal 88:3392-3397.